J. Phys.: Condens. Matter **25** (2013) 306001 (9pp) doi:10.1088/0953-8984/25/30/306001

A TDPAC study of static and dynamic magnetic behaviour

T A Webb and D H Ryan

Physics Department and Centre for the Physics of Materials, McGill University, 3600 University Street, Montreal, QC, H3A 2T8, Canada

E-mail: webbt@physics.mcgill.ca

Received 29 April 2013, in final form 11 June 2013
Published 3 July 2013
Online at stacks.iop.org/JPhysCM/25/306001

Abstract
The a-Fe_xHf_{100-x} system is used to explore the application of TDPAC (the time differential perturbed γ–γ angular correlation technique) to non-trivial anisotropic magnetic relaxation. The effect of fluctuations in this system is primarily to cause a decay of the zero-frequency component, which is characterized by the phenomenological decay rate λ. The zero-field magnetic phase diagram, constructed from both static and dynamic features of the data, and the temperature dependence of λ are both fully consistent with the physics of partial bond frustration. The results demonstrate that the magnetic fluctuations are meaningfully characterized by simple spectrum features, and are not obscured by large static fields or severe disorder.

(Some figures may appear in colour only in the online journal)

1. Introduction

In contrast to many other techniques, the time differential perturbed γ–γ angular correlation technique (TDPAC) has a sensitivity to dynamics that allows it to be used to unambiguously distinguish the effects of dynamic relaxation from those due to static disorder. The technique measures the γ emission anisotropy for an ensemble of nuclei selected by the detection of a previously emitted γ-ray. The γ–γ angular correlation has a 'hard core' associated with correlations which persist at long times and do not time average to zero [1, 2]. The typical TDPAC pattern for a magnetic interaction (figure 1(a)) is visually dominated by an oscillatory signal, but also contains a time-independent, zero-frequency component, a_0, shown by the dashed line. This zero-frequency component reflects the persisting correlations and sets a lower limit on the time-integrated angular correlation: the hard core [1]. Adding a static distribution of local environments smears out the regular precession signal but does not affect the hard core, as can be seen in figure 1(b) [3]. Indeed, the hard core contribution can only be diminished in the presence of dynamics [2], and the shape of the corresponding decaying zero-frequency component contains information about the symmetry of the fluctuations [4]. For example, in the case of slow isotropic rotational diffusion (figure 1(c)), treated by Marshall and Meares [5], the zero-frequency component decays to zero, while a magnetic field (B) which fluctuates between $+z$ and $-z$ orientations will produce no decay in the zero-frequency component (figure 1(d)) because the fluctuations do not cause a mixing of the energy eigenstates. More generally, a time-dependent hyperfine interaction Hamiltonian which is diagonalizable at all times by the same set of static eigenstates will never produce a decaying zero-frequency component [6], but rather leads only to a smearing or damping of the oscillating components in much the same way as static disorder (compare figures 1(b) and (d)). Conversely, the observation of a decaying zero-frequency component unambiguously signals the presence of dynamic fluctuations that mix the energy eigenstates.

As a technique of time-domain measurement of nuclear precession, TDPAC does not require the use of an applied field to study magnetic systems. Despite the richness of information available from this local, zero-field technique and success in characterizing magnetic fluctuations (notably demonstrated in the study of critical phenomena [8, 9]), TDPAC is not often used to study magnetic dynamics, in contrast to the muon spin relaxation technique (μSR), another technique of time-domain measurement of emission anisotropy with a similar sensitivity to dynamic interactions.

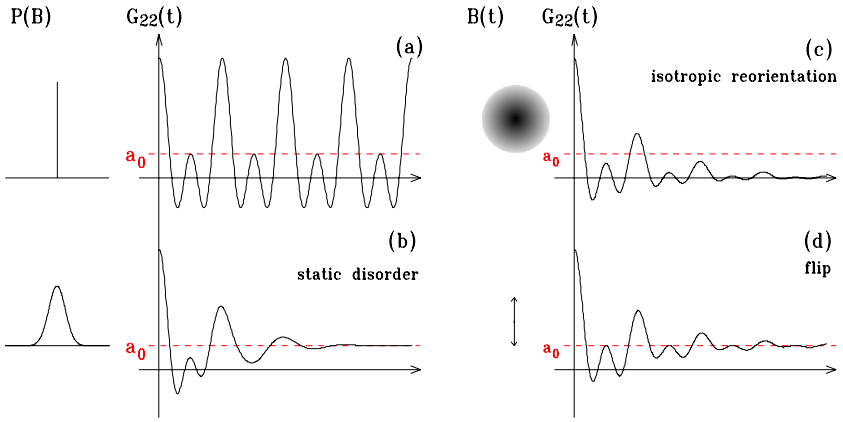

Figure 1. Comparison of the TDPAC powder perturbation factor G_{22} for a magnetic dipole interaction of an $I = 5/2$ probe with typical static and dynamic field environments. The zero-frequency component for the static case, a_0, is shown as a dashed line on each panel. (a) A single static field; (b) a static Gaussian distribution of fields [3]; (c) a field whose orientation diffuses isotropically over all possible directions [5]; (d) a field that flips between two antiparallel directions (calculated using SHIML [7]). Note that only the rotationally diffusing field (c) leads to a decay of the zero-frequency component.

As spin-$\frac{1}{2}$ particles, muons are sensitive only to the local magnetic field (and not to the electric field gradient—EFG) [10], making them useful probes of magnetism; however, μSR requires access to a major user facility while TDPAC can be carried out as an in-house benchtop-scale experiment.

The general problem of γ–γ angular correlations perturbed by a time-dependent interaction is not easily solved. Limiting forms in cases of high symmetry are well-established [2, 5, 11, 4, 12], but such analytic approximations are generally limited to instances of high symmetry, long measurement times, small perturbations, or a combination thereof. The more versatile Blume stochastic modelling, as described by Winkler and Gerdau [6], is computationally intensive. However, computational limitations are becoming less important with modern computers, and systematic studies have demonstrated for electric field gradient (EFG) fluctuations that stochastic modelling can provide a quantitative link between phenomenological features in TDPAC spectra and the underlying dynamic processes [13–15].

Most applications of TDPAC to dynamics have focused on fluctuations in the EFG[1], and as the two most common TDPAC probes, ^{111}Cd and ^{181}Ta, are non-magnetic species they typically see magnetism superimposed on the effects of the EFG, such that magnetic fluctuations present a non-trivial low symmetry problem that is not described in any detail by the theoretical models that have been developed to date. In order to motivate further development of useful models, we set out to investigate what information can be extracted about magnetic fluctuations from a TDPAC spectrum. We focus here on the dynamic features, particularly the shape of the zero-frequency component, of TDPAC spectra in a system with fluctuating magnetic fields. As the role of TDPAC in studying magnetic dynamics has largely gone unexplored, we use a model system that has been characterized by other methods and is therefore reasonably well understood: Fe-rich a-Fe$_x$Hf$_{100-x}$ metallic glasses, which exhibit magnetic fluctuations with well-known behaviour, and into which the ^{181}Hf probe is easily introduced by neutron activation.

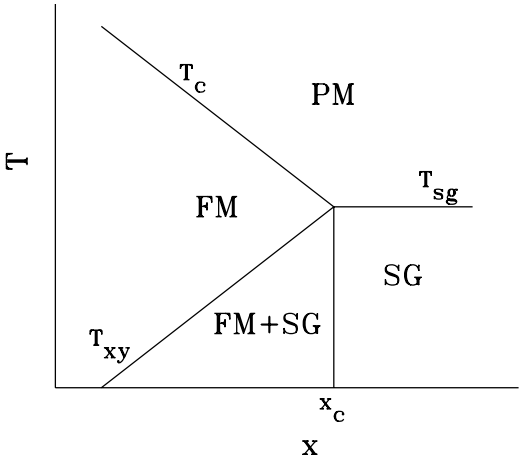

Figure 2. Generic phase diagram for partially bond-frustrated systems. For frustration below x_c, ferromagnetic (FM) order appears at T_c, followed by transverse spin freezing at T_{xy}. Above x_c, a single transition to an SG occurs.

The Fe–Hf system is one of a larger class of partially bond-frustrated materials which can exhibit coexisting ferromagnetic and xy-spin-glass (SG) ordering depending on the level of frustration (figure 2). In Fe–T (T = early transition metal) glasses, the distribution in Fe–Fe separations produces competing ferromagnetic (FM) and antiferromagnetic (AF) interactions as a result of the change in sign of the Fe–Fe direct exchange. The level of frustration can be tuned by adjusting the chemistry: adding larger Hf/Zr atoms results in more FM interactions [16]. The magnetic phase diagram has been mapped out both numerically with Monte Carlo simulations of a $\pm J$ Heisenberg spin model [17], and experimentally for Fe-rich a-Fe$_x$Zr$_{100-x}$ and related systems [18]. At lower levels of frustration, the onset of FM

[1] For example, refer to the work of Forker *et al* [14] which includes a brief review of dynamics in TDPAC in the introduction.

order at T_c is followed by freezing of the transverse (x, y) spin components to form a coexisting xy-SG. The pre-existing FM order is unaffected by the onset of non-collinearity; below T_{xy}, long-range FM and SG order coexist [19]. However, above a critical level of frustration at x_c, ferromagnetic order ceases to form, and a single transition is observed from the paramagnetic phase to a three-dimensional SG [20, 21].

Both magnetic transitions at T_c and at T_{xy} are accompanied by spin fluctuations, predicted by simulations [22] and observed by both μSR [18] and the selective excitation double Mössbauer technique (SEDM) [23] in the Fe–Zr system. We therefore expect, on the basis of similarities to the Fe–Zr system [19, 24–26], the Fe–Hf system to provide slow (∼10 MHz [23]) dynamic magnetic interactions in two regimes: in the presence of a large static magnetic field at T_{xy} and in the presence of a negligible static magnetic field near T_c, allowing us to evaluate our models in two important limits.

The TDPAC spectra show a clear reduction in the hard core, and comparison to the Zr-based system provides a firm platform for analysis of the corresponding zero-frequency component decay. With a simple phenomenological parametrization of the spectra, TDPAC is able to characterize not only the fluctuations at T_c, but also those at T_{xy}, which in many techniques are obscured by the dominant ferromagnetic order, demonstrating a meaningful qualitative link between simple spectrum features and the physics in these materials, despite the complexity of the theoretical relaxation problem.

2. Experimental methods

a-Fe_xHf_{100-x} samples were prepared near the $x = 92.1$ at.% eutectic by arc-melting stoichiometric quantities of the pure elements (Fe 99.97%, Hf 99.9%) under an argon atmosphere, followed by melt-spinning on a copper wheel in helium, with an argon ejection gas and tangential wheel speed of roughly 50 m s^{-1}. The Fe, Hf and Zr contents were then measured by wavelength dispersive spectroscopy (WDS) microprobe analysis on a JXA JEOL-8900L instrument with acceleration voltage 20 kV, beam current 20 nA and beam size 10 μm. Three WDS analyses were performed at different locations on the free side of the ribbons for each sample, and showed variations in Fe content near 0.1 at.%. The average of the three measurements gave Fe concentrations $x = 91.3$, 91.7 and 91.9 at.% for the samples reported here, and the Zr content ranged from 0 to 3 at.% of the combined Hf and Zr content in individual analyses. In general, the compositions showed a tendency to be closer to the eutectic composition than the nominal values. An $x = 92.1$ at.% sample prepared similarly was obtained from earlier work (previously reported at the nominal value 92.5 at.%) [19].

X-ray diffraction of both the free and wheel sides revealed smooth broad peaks, consistent with amorphous structure, and room temperature Mössbauer spectra showed no evidence for crystalline impurities.

^{57}Fe Mössbauer spectra of the $x = 91.3$, 91.7, 91.9 at.% samples were collected down to 18 K in a closed-cycle helium refrigerator to extract the hyperfine field (B_{hf}) at Fe sites. Mössbauer results for the $x = 92.1$ at.% sample were previously reported by Ren *et al* [19]. Spectra were fitted to a Gaussian distribution of quadrupole splittings with a linear correlation between isomer shift and quadrupole splitting above T_c, and to an asymmetric Gaussian distribution in B_{hf} below T_c, with a linear correlation between isomer shift and B_{hf}.

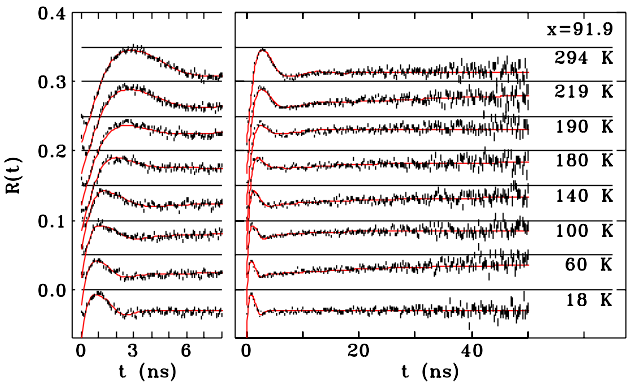

Figure 3. Representative TDPAC spectra of a-$Fe_{91.9}Hf_{8.1}$, showing short-time behaviour on the left and long-time behaviour on the right. Solid lines through the data are fits described in the text. The horizontal lines indicate the zero of each spectrum.

Pieces of the melt-spun ribbons (5–10 mg Hf content) enclosed in quartz tubes were irradiated in a neutron flux (1.1×10^{13}n cm^{-2} s^{-1} nominal) at the McMaster Nuclear Reactor to produce ^{181}Hf activity. Irradiation times ranged from 45 min to 2 h, producing sample activities from 0.5 to 1.5 MBq. TDPAC spectra using the $^{181}Hf \rightarrow {}^{181}Ta$ decay were collected on a digital spectrometer [27] from room temperature down to 18 K (261–23 K for the $x = 92.1$ at.% sample) using a closed-cycle helium refrigerator. Preliminary results for $x = 91.7$ at.% (nominally 91 at.%) have already been reported [28].

3. TDPAC data and analysis

Representative TDPAC spectra of a-$Fe_{91.9}Hf_{8.1}$ are shown in figure 3. The broad static distribution of local environments associated with the amorphous structure means that oscillatory components are damped rapidly at all temperatures, leaving only the zero-frequency component at long times. At room temperature, the sample is paramagnetic, and the observed spectrum is described by a broad distribution in quadrupole frequencies. Oscillations are visible in the first 10 ns of the spectrum. As the sample is cooled and magnetic order develops, the oscillation timescale is reduced to approximately 3 ns, as higher frequencies are introduced by the growing magnetic interaction.

The spectra were fitted to

$$R(t) = A_{22}G_{22}(t), \tag{1}$$

using the first 40 ns of data. Several modifications to the standard polycrystalline perturbation factor were required (see for example the review by Frauenfelder and Steffen [1]). For

static interactions,

$$G_{22}^{(s)}(t) = a_0 + \sum_{i=1}^{3} a_i f(\omega_i, t)\cos(\omega_i t). \quad (2)$$

Inside the sum, $f(\omega_i, t)$ consists of two factors to account for both the finite time resolution [29] and the damping due to disorder [3]. The latter factor has the form $\exp[-\frac{1}{2}(2-\alpha)(\delta_i\omega_i t)^{1+\alpha}]$, where α interpolates between Gaussian ($\alpha = 1$) and Lorentzian ($\alpha = 0$) distributions in the contributing frequencies.

We also expect time-dependent interactions due to magnetic fluctuations, and correspondingly, a decay appears in the zero-frequency component of the TDPAC spectra at intermediate temperatures. The trend is clearly visible in the 18–60–100 K spectrum sequence of figure 3 for larger values of t, after the oscillatory components have been fully damped ($t > 10$ ns).

In the case of isotropic fluctuations, the perturbation factors can be approximated by

$$G_{kk}(t; \omega_{Q/L}, \tau_c) = e^{-\lambda_k t} G_{kk}^{(s)}(t; \omega_{Q/L}), \quad (3)$$

where λ_k describes the rate of relaxation to an isotropic angular distribution, τ_c is the correlation time for the dynamic physical process, and $G_{kk}^{(s)}$ is the theoretical form for a static interaction of strength ω_Q (electric) or ω_L (magnetic). This product form can be applied in two regimes.

(i) For slow ($\omega\tau_c \ll 1$) isotropic reorientation of fields, $G_{kk}^{(s)}(t)$ describes the instantaneous distribution of probe environments, and λ_k increases as fluctuations become more rapid [5].

(ii) For rapid fluctuations, where $t \gg \tau_c$ and $\omega^2 t\tau_c \ll 1$, the effect is motional averaging: $G_{kk}^{(s)}(t)$ describes the time-averaged interaction at probe sites, and λ_k *decreases* as the fluctuations become more rapid [2, 4].

More general forms, which do not necessarily assume isotropic fluctuations, can contain multiple exponentials, and the decay rates do not have to be identical for each of the oscillating components [6, 4, 11]. Here in the Fe–Hf system, the dominant source of damping for the oscillatory components is the static disorder, as will be discussed in more detail in section 6, so the effect of dynamics on the sum in (2) is of minimal importance, with the result that the surviving effects of dynamics are seen primarily in the behaviour of a_0. In order to reproduce the observed behaviour of the zero-frequency component at long times, a combination of decaying and non-decaying fractions was required:

$$G_{22}(t) = \left[a_e e^{-\lambda t} + (1 - a_e)\right] G_{22}^{(s)}(t) \quad (4)$$

was used to fit the spectra. Introducing multiple exponentials did not improve the fits, and the decay rates derived from multi-exponential fits were not well defined. It can be seen from the example spectra in figure 3 that the phenomenological product form shown in (4) describes the data quite well.

As the interactions with the EFG and with B_{hf} are of comparable strength [28], a numerical diagonalization of the hyperfine interaction Hamiltonian was used to calculate the frequencies (ω_i) and powder intensities (a_i) from B_{hf} and the EFG, parametrized by the quadrupole frequency ω_Q and the axial asymmetry η. Because the local magnetic order is not expected to be correlated with the local structure, a 500-point Monte Carlo average over the orientation of B_{hf} with respect to the EFG was performed, and the strength of the EFG and B_{hf} were allowed to have different distribution widths, characterized by dimensionless parameters δ_Q for the EFG and δ_B for B_{hf}, as previously described [28].

The heavy damping of spectra made careful restriction of the number of free parameters essential. For each spectrum, four or five parameters were refined, with the others fixed as follows.

- Instrument-dependent parameters (the effective angular correlation coefficient A_{22}, the timing resolution τ, and the time origin t_0) were fixed for each sample from the lowest temperature spectrum, assuming no dynamics ($\lambda = 0$), with the exception that for $x = 91.3$ at.%, t_0 was fixed from the room temperature spectrum, as the 19 K spectrum favoured an unusually large value of t_0.
- The axial asymmetry of the EFG, η, was fixed from the highest temperature spectrum.
- If B_{hf} and δ_B were refined, ω_Q and δ_Q were fixed from the highest temperature spectrum.
- Below T_c, α was fixed to 1.0.

4. Results

Parameters describing the room temperature paramagnetic state and the low temperature magnetic state are listed in table 1. The EFG parameters ω_Q, δ_Q and η from the highest temperature spectrum for each sample are similar, reflecting minimal changes in the Hf environment of the paramagnetic phase as the composition of the glass evolves. Note that the values for $x = 92.1$ at.%, which differ from those for the other three compositions, were obtained at a lower temperature. B_{hf} and δ_B derived from the lowest temperature spectra also show similar Hf environments in the magnetically ordered phase. These observations are consistent with a constant glass structure over the narrow composition range covered here.

The temperature dependence of the average B_{hf} at Hf sites from TDPAC and at Fe sites from Mössbauer spectroscopy, shown in figure 4, were fitted to Brillouin functions modified for disorder [30]. Low temperature data were excluded from the fits, as will be discussed. The extracted values for T_c (table 2) increase with Hf content, and show excellent agreement between the TDPAC and Mössbauer data. At low temperatures, the data show a stronger temperature dependence than the modified Brillouin function, consistent with the ordering of additional spin components at the transverse spin freezing transition [18]; however, the break in behaviour is not sufficiently well defined to permit estimates for T_{xy} to be extracted, in contrast to the case for μSR used to study the Zr-based series [18]. The low temperature break

Table 1. EFG parameters extracted from the highest (H) temperature spectrum (261 K for $x = 92.1$ at.%, room temperature otherwise) and magnetic parameters from the lowest (L) temperature spectrum for each a-Fe_xHf_{100-x} sample.

x (at.%)	$\omega_Q^{(H)}$ (Mrad s^{-1})	$\delta_Q^{(H)}$	$\eta^{(H)}$	$B_{hf}^{(L)}$ (T)	$\delta_B^{(L)}$
91.3	85(7)	0.36(4)	0.62(4)	13(1)	0.27(3)
91.7	94(4)	0.34(1)	0.48(1)	13(1)	0.32(3)
91.9	92(4)	0.31(1)	0.53(1)	13(1)	0.28(3)
92.1	113(4)	0.35(2)	0.27(1)	12(1)	0.28(3)

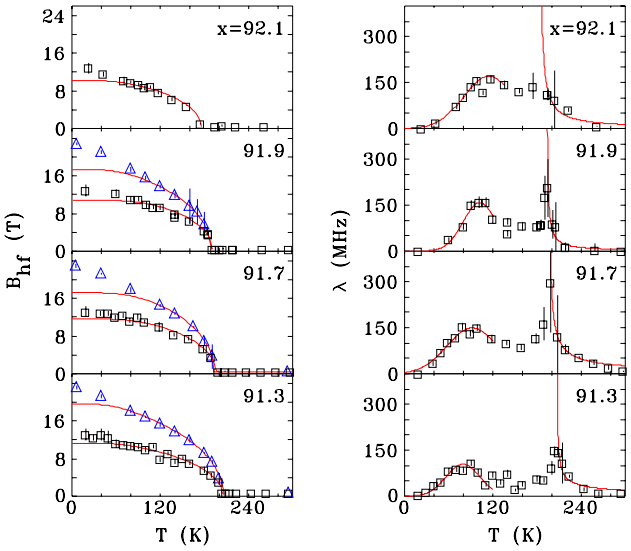

Figure 4. *Left:* average B_{hf} at Fe sites from Mössbauer spectra (triangles) and at Hf sites from TDPAC spectra (squares). Lines are fits to Brillouin functions modified for disorder. *Right:* TDPAC spectrum decay rate showing two peaks associated with the onset of magnetic order at T_c and transverse spin freezing at T_{xy}.

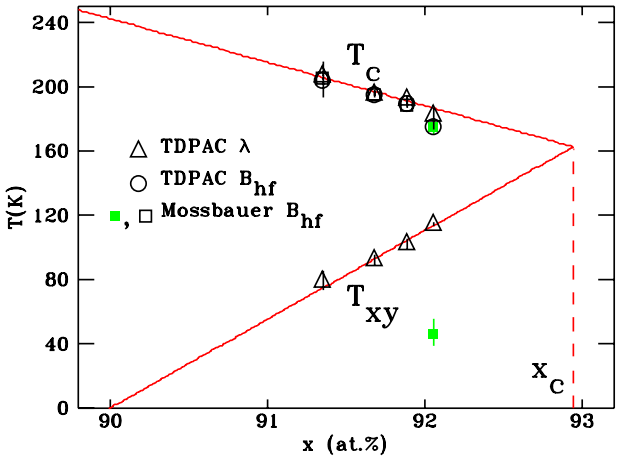

Figure 5. a-Fe_xHf_{100-x} zero-field magnetic phase diagram showing TDPAC and Mössbauer results from this work (open symbols), and the Mössbauer results (solid symbols) of Ren *et al* [19] for $x = 92.1$ at.%. Lines are fits to T_c and T_{xy}.

Table 2. Ferromagnetic ordering temperatures T_c and transverse spin freezing temperatures T_{xy} for a-Fe_xHf_{100-x} samples, extracted from the decay rate of TDPAC spectra (λ), the average B_{hf} at Hf sites (TDPAC) and the average B_{hf} at Fe sites (Mössbauer).

x (at.%)	T_{xy} (K) λ	T_C (K) λ	T_C (K) B_{hf}(Hf)	T_C (K) B_{hf}(Fe)
91.3	79(6)	207(1)	205(11)	205.4(4)
91.7	92(3)	196(1)	195(2)	195(1)
91.9	102(3)	193(5)	190(4)	189(2)
92.1	114(1)	182(4)	175(2)	175(5) [19]

in behaviour is more pronounced in the ^{57}Fe Mössbauer data as the behaviour of the Fe moments is probed both locally and directly, in contrast to the TDPAC-derived fields at the Hf sites, which are both more remote and also reflect an average over contributions from several Fe first neighbours.

The observed spectrum relaxation is characterized by the rate λ. The temperature dependence (figure 4) strongly resembles that of the μSR dynamic relaxation rate from work on the Fe–Zr series [31, 18]. A sharp peak occurs at the onset of magnetic order, and a smooth, broad peak at a lower temperature roughly coincides with the break from Brillouin behaviour in B_{hf}, where transverse spin freezing is expected. Estimates for T_c and T_{xy} were therefore extracted by fitting the high and low temperature features to an inverse power law and a Gaussian peak (curves in figure 4), respectively, and are listed in table 2. The two features move farther apart with increasing Hf content, and the T_{xy} peak becomes more diffuse; a similar trend is visible in the μSR data of Ryan *et al* [32].

5. Comparison to a-Fe_xZr_{100-x}

The results are summarized in the magnetic phase diagram of figure 5. T_c decreases at 27(2) K/at.% and T_{xy} increases at 55(7) K/at.% from $x = 91.3$ to 92.1 at.%, indicating increasing frustration, as expected. The values of T_c are larger than those previously reported by Ryan *et al* based on bulk magnetization measurements [33], but show a similar dependence on Hf content. Linear extrapolation places an estimate for x_c at ~93 at.%, and indicates that non-collinear order should cease to form below 90 at.% Fe, slightly larger than the Fe content with maximum T_c reported at 87 at.% in sputtered alloys by Liou *et al* [24]. Note that T_c has been observed to steepen significantly near x_c in numerical simulations of the $\pm J$ Heisenberg spin model [21], and experimentally in both a-Fe_xZr_{100-x} and a-$Fe_{90-x}Ru_xZr_{10}$ [18]. The linear approximation may therefore tend to overestimate both x_c and the corresponding spin-glass transition temperature. Over the range studied (91.3–92.1 at.%), T_c is indistinguishable from the that of the Zr-based system [18], and T_{xy} is slightly higher (~10 K). An estimate of T_{xy} for $x = 92.1$ at.% had previously been derived from 3.5 T applied field Mössbauer spectra [19] and

is included in figure 5 for comparison. The applied field T_{xy} at 47(8) K is strongly suppressed from the 114(1) K obtained by TDPAC, underscoring the value of TDPAC as a zero-field technique. Furthermore, the field suppression of T_{xy} seen here ($T_{xy}(3.5\ \mathrm{T})/T_{xy}(0) = 0.41(7)$) is fully consistent with the value of 0.51(6) seen by using μSR in a-$Fe_{92}Zr_8$ in the same field [34].

In the $\pm J$ Heisenberg spin model, the level of frustration can be parametrized by the ratio of AF bonds to FM bonds, as the exchange constant between two sites can take on only one of two values: $+J$ (FM) or $-J$ (AF). Quantifying frustration is more complex in a-Fe_xT_{100-x} materials, where a continuous distribution is expected, and where the variation in Fe environments also leads to a distribution in the strength of the Fe moments [35]. The strong resemblance of the numerical [17] and experimental [18] phase diagrams suggests that frustration is closely related to the Fe concentration, x, and that frustration has a characteristic simultaneous effect on T_c and T_{xy}. The correspondence between the composition dependences of the two transition temperatures is therefore a strong indication that our TDPAC λ-derived T_{xy} is correctly identifying the transverse spin ordering event. From the strong chemical similarity of Hf to Zr and their similar atomic radii [26, 36], we expect the a-Fe–Hf and a-Fe–Zr systems to have similar distributions in Fe moments and Fe–Fe spacings, in agreement with the observed similarity between their magnetic phase diagrams.

6. Discussion of TDPAC analysis

The decay of the zero-frequency component in the TDPAC spectra is a clear signature of dynamic interactions, which we associate with the Fe magnetic moment fluctuations arising from bond frustration. The presence of the non-decaying component, $(1 - a_e)$ in (4), can be linked to anisotropy of the time-dependent hyperfine interaction Hamiltonian. Random isotropic interactions will always produce a relaxation to zero (isotropic distribution of γ_2), whereas fluctuations which do not mix the static energy eigenstates will introduce no time-dependent attenuation of the zero-frequency component [6]. The value of a_e is approximately 0.5 for all compositions, and is relatively temperature independent, implying independence of the time-averaged B_{hf} (static component). This observation suggests that a_e reflects behaviour in either the fluctuating component of the local field, or the static temperature-independent structure (EFG). The former is corroborated by the findings of Andrade *et al* [4] that the time dependence of the zero-frequency component reflects the symmetry of the fluctuating component. However, this comparison is limited as their work assumes an axially symmetric static interaction and measurement times much larger than the correlation time associated with the fluctuations ($t \gg \tau_c$), whereas if we assume, on the basis of the similarity to the Fe–Zr system, that the Fe moment fluctuation rate is roughly 10 MHz, then $\tau_c \approx 100$ ns and the TDPAC spectra are in the regime $t < \tau_c$. The 10.8 ns half-life of the ^{181}Ta γ–γ cascade intermediate state precludes collecting spectra with a good signal to noise ratio at times larger than τ_c (ten half-lives). From our data, we therefore cannot conclusively eliminate the possibility of relaxation to zero at much longer times ($\sim\mu$s).

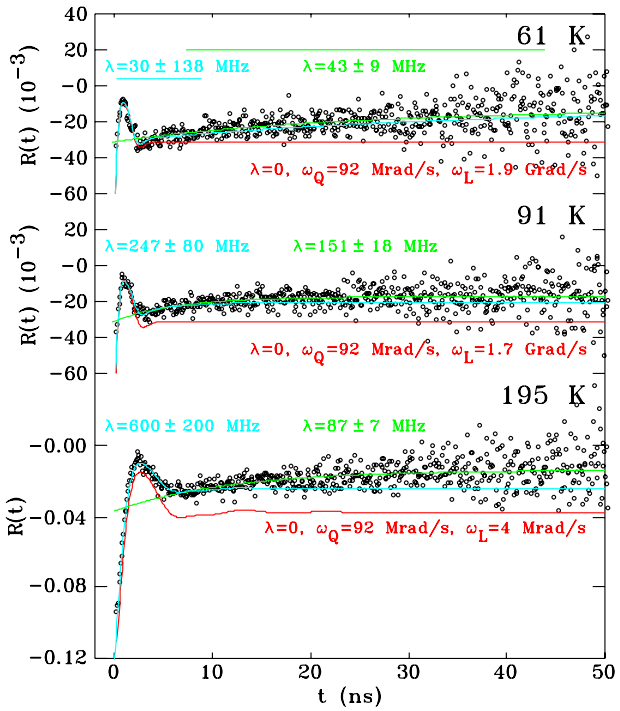

Figure 6. TDPAC spectra of a-$Fe_{91.9}Hf_{8.1}$ near T_c (195 K, bottom), near T_{xy} (91 K, middle) and below T_{xy} (61 K, top), with static behaviour described by the $\lambda = 0$ curves. The remaining curves characterize the behaviours at short and long time with the indicated values of λ obtained by fitting the ranges of data indicated by horizontal bars at the top. Data deviate from static behaviour on both timescales near T_c but not at lower temperatures. Error bars on the points have been left out for clarity.

The product form, (4), used to fit the data is appropriate for dynamic features appearing on longer timescales than static features, which can result from either very slow or very rapid fluctuations, i.e. regimes i and ii for (3). Examination of τ_c estimated above ($\sim$100 ns) and ω_Q ($\sim$100 Mrad s^{-1}, table 1) indicates that the fluctuations in this system are slow and therefore that an increase in λ corresponds to an increasing fluctuation rate. The consistency in the temperature dependence of λ with the μSR and SEDM magnetic relaxation rates in the Fe–Zr system strongly confirms this relationship. In order to achieve the separation of static and dynamic spectrum features appropriate for the product approximation, the fluctuation rate ($\sim\tau_c^{-1}$) must be much slower than ω_L or ω_Q. As a result, (4) is a poor description of the TDPAC spectra near T_c, where the static B_{hf} is small or negligible, and the fluctuation rate is diverging. The separation in time between the rapid oscillations (ω_i, (2)) and the slow decay (λ) is lost.

We examine in detail the 195 K spectrum of a-$Fe_{91.9}Hf_{8.1}$ (figure 6) as an example of the observed behaviour just above T_c. Under the assumption of slow fluctuations, the parameters ω_Q, δ_Q, B_{hf} and δ_B in $G_{22}^{(s)}(t)$ characterize the instantaneous distributions in EFG and B_{hf} at any given time, i.e. the system in the absence of fluctuations. $G_{22}^{(s)}(t)$ (the $\lambda = 0$ curve in

the bottom panel of figure 6) is therefore a static model used to characterize oscillatory behaviour in the spectrum as being due to the underlying *static* distributions in probe environments. Closer examination reveals that the data not only show a slow decay in the zero-frequency component at late times, but also exhibit a much sharper rise at early times. Fitting the first 9 ns of data to (4) gives a large value for λ of 600 $\pm$ 200 MHz, compared to only 87(7) MHz obtained from a fit to the long-time decay[2]. In contrast, near T_{xy} (91 K, middle panel of figure 6) and below T_{xy} (61 K, top panel of figure 6), the short-time fit does not deviate significantly from $G_{22}^{(s)}(t)$ until the oscillations have mostly damped out: static disorder is the dominant source of damping. The same cannot be said for near T_c, where the data deviate from static behaviour on both short and long timescales. Near T_c, the significant contribution from the EFG becomes more important, and the disorder (both in magnitude and direction) makes it difficult to distinguish the effects of dynamics from those of the underlying, static, frequency distribution (ω_i in (2)).

A close analogy can be drawn between TDPAC and μSR. For the Fe-rich amorphous Fe–Hf and Fe–Zr compounds, the signals from the static and dynamic behaviours are segregated into the short and long times of spectra, respectively, in both techniques. However, the timescale separation in TDPAC is less pronounced than in μSR, being only an order of magnitude near T_{xy} (compared with almost three orders of magnitude in μSR [18]) and disappearing near T_c. Furthermore, the static behaviour is more complex due to TDPAC's sensitivity to the EFG. Nonetheless, we observe the same qualitative temperature dependence of the dynamic relaxation rate (λ here), showing signatures of both T_c and T_{xy}, confirming the assignment of features in λ to the magnetic ordering events at T_c and T_{xy} and the interpretation of λ as a description of fluctuations in the slow dynamics regime. However, a quantitative comparison between the TDPAC and μSR results cannot be made. The dynamic relaxation rate in μSR is the fluctuation rate for the local magnetic field at the location of the muon within the sample, extracted by fitting spectra to a model of Markovian isotropic relaxation [18]. The ^{181}Ta TDPAC probe, however, sees magnetism superimposed on a static EFG, breaking any isotropy in the magnetism that might be exploited to simplify calculations. Moreover, the disorder associated with the distribution in EFGs and the fact that they are uncorrelated with the magnetism introduces so many parameters that any realistic physical model is computationally unfeasible. We are therefore unable to unambiguously relate λ to a timescale associated with a physical process. In fact, the relationship between λ and the physical rate is likely to depend on the static fields present [37, 13], and therefore almost certainly changes between T_{xy} and T_c. However, we do not know the size of this effect.

Further theoretical work is required to move beyond the limitations discussed above: understanding the non-decaying component ($1 - a_e$), describing spectrum features near T_c, and relating λ to a magnetic fluctuation rate. Numerical simulations using the Blume stochastic model have the advantage of not being restricted by the need for simplifying assumptions that are often essential for making analytical solutions possible. They can therefore be used to calculate perturbation factors for any combination of interaction strength (ω) and correlation time (τ_c) and should permit the relationship between the underlying spin fluctuation rate and the value of λ observed in the decay of the zero-frequency component to be determined in simpler systems. This versatility has been demonstrated by the success of stochastic modelling in finding and characterizing meaningful parametrizations, in evaluating regimes in which approximations are valid, and in identifying potential ambiguities or systematic errors in parameter interpretation [37, 14, 13, 38, 15]. Systematic studies of simplified models may therefore provide the missing insight into the connection between physics and phenomenology in the case of magnetic fluctuations. Of particular interest here are (i) the influence of the symmetry of both static and fluctuating field components on the zero-frequency decay, and (ii) how static interactions and disorder influence λ's dependence on the magnetic relaxation rate. A physical understanding of the TDPAC data is necessary in order to make a concrete quantitative comparison to other techniques.

7. Conclusions

a-Fe$_x$Hf$_{100-x}$ is a complex system for TDPAC. Time-dependent magnetic interactions, due to fluctuations in B_{hf}, are superimposed on independent and disordered static electric quadrupole and magnetic dipole interactions. Damping by the static disorder confines oscillations to the first 10 ns of spectra, while the decay of the remaining zero-frequency component provides a clear signature of the dynamics, which is not obscured by the large static magnetic field at T_{xy}.

We demonstrate that we are indeed observing the physics of bond-frustrated materials.

- The static and dynamic features of the TDPAC data at the transition temperatures are fully consistent with the Mössbauer work on the same samples, and with studies of the Zr-based system.
- The zero-field magnetic phase diagram is almost indistinguishable from that of a-Fe–Zr, in agreement with previous studies of magnetic and structural properties of these materials.

On this basis, a comparison is made between features of TDPAC data and descriptions of T_c and T_{xy} by other techniques. We conclude that λ meaningfully characterizes the magnetic fluctuation rate. Previous theoretical work suggests that with a better understanding of how the symmetry of static and fluctuating fields affects the zero-frequency component, the non-decaying fraction might reveal information about the relaxation mechanism.

In the product approximation used, λ and a_e characterize features of the zero-frequency component which are

[2] For the large t fit, ω_Q, δ_Q, B_{hf} and δ_B from the fit described in section 3 were used, as these values are not well defined from this data range. The curve shown in figure 6 is only the exponential factor.

visible by eye in the spectra. The approach taken—to identify meaningful features in TDPAC spectra, a minimal parametrization and the regime of its applicability—demonstrates the value in phenomenology. However, a comprehensive description of effects due to dynamic magnetic interactions is unrealistic, and attempts to extract too much information with a 'complete' description threaten to produce ambiguous results from the inevitable proliferation of adjustable parameters.

Theoretical and numerical investigations are needed to develop physical interpretations, as quantitative comparison to other techniques is essential, both in order to confirm the interpretation of spectrum features and to further exploit the complementarity of information.

It may be possible to reduce the complexity that has made a physical model intractable in this case, for example by: (i) working with a crystalline system in which the static structural and magnetic order are fixed with respect to the crystallographic axes; (ii) placing the probe nuclei in a cubic environment where the EFG is zero; (iii) using a TDPAC probe nucleus that has a much smaller nuclear quadrupole moment, such as ^{140}Ce, so that the magnetic contribution is dominant.

Application of TDPAC to magnetic dynamics is promising in terms of sensitivity to both the relaxation rate and the mechanism. Theoretical and experimental investigations of the link between the quantum mechanical relaxation problem and TDPAC spectrum phenomenology are essential for fully exploiting the technique.

Acknowledgments

This research was supported by grants from the Natural Sciences and Engineering Research Council of Canada and Fonds Québécois de la Recherche sur la Nature et les Technologies. Neutron activation was carried out by M Butler at the McMaster Nuclear Reactor (MNR), Hamilton, Ontario. The a-$Fe_{92.1}Hf_{7.9}$ sample was made by Hong Ren (McGill). WDS was performed by Lang Shi at the McGill University Microprobe Laboratory. TAW would like to thank M O Zacate of the Department of Physics & Geology, Northern Kentucky University, for useful discussions.

References

[1] Frauenfelder H and Steffen R M 1965 *Alpha-, Beta-and Gamma-Ray Spectroscopy* (Amsterdam: North-Holland) p 997
[2] Abragam A and Pound R V 1953 Influence of electric and magnetic fields on angular correlations *Phys. Rev.* **92** 943–62
[3] Rogers J D and Vasquez A 1975 Data reduction in perturbed angular correlation experiments *Nucl. Instrum. Methods* **130** 539–41
[4] da P, Andrade R, Rogers J D and Vasquez A 1969 Influence of simultaneous static and time-dependent quadrupole interactions on gamma–gamma angular correlations *Phys. Rev.* **188** 571–5
[5] Marshall A G and Meares C F 1972 Effect of slow rotational diffusion on angular correlations *J. Chem. Phys.* **56** 1226–9
[6] Winkler H and Gerdau E 1973 $\gamma\gamma$-angular correlations perturbed by stochastic fluctuating fields *Z. Phys.* **262** 363–76
[7] Zacate M O and Evenson W E 2011 Stochastic hyperfine interactions modeling library *Comput. Phys. Commun.* **182** 1061–77
[8] Collins G S, Chowdhury A R and Hohenemser C 1986 Observation of isotropic critical spin fluctuations in Gd *Phys. Rev.* B **33** 4747–51
[9] Hohenemser C, Rosov N and Kleinhammes A 1989 Critical phenomena studied via nuclear techniques *Hyperfine Interact.* **49** 267–324
[10] Schatz G and Weidinger A 1996 *Nuclear Condensed Matter Physics: Nuclear Methods and Applications* 2nd edn (Chichester: Wiley)
[11] Dillenburg D and Maris Th A J 1962 The effect of statistical perturbations on angular correlations *Nucl. Phys.* B **33** 208–17
[12] Micha D A 1967 Perturbation of angular correlations by randomly oriented fluctuating magnetic fields *Phys. Rev.* **156** 627–30
[13] Evenson W E, Gardner J A, Wang R, Su H-T and McKale A G 1990 PAC analysis of defect motion by Blume's stochastic model for $i = 5/2$ electric quadrupole interactions *Hyperfine Interact.* **62** 283–300
[14] Forker M, Herz W and Simon D 1994 Approximation of the theory of stochastic perturbations of angular correlations for fluctuating distributions of electric quadrupole interactions *Nucl. Instrum. Methods Phys. Res.* A **337** 534–43
[15] Castle J R, Zacate M O and Evenson W E 2013 Realistic models of stochastically varying hyperfine interactions caused by vacancy diffusion in $L1_2$-structured compounds *Hyperfine Interact.* **222** 109–20
[16] Ryan D H 1992 *Recent Progress in Random Magnets* (Singapore: World Scientific) chapter 1, pp 1–40
[17] Beath A D, Ryan D H, Cadogan J M and van Lierop J 2012 Field dependence of the transverse spin glass phase transition: quantitative agreement between Monte Carlo simulations and experiments *J. Appl. Phys.* **111** 07E108
[18] Ryan D H, van Lierop J and Cadogan J M 2004 Zero-field muon spin relaxation studies of frustrated magnets: physics and analysis issues *J. Phys.: Condens. Matter* **16** S4619–38
[19] Ren H and Ryan D H 1995 Exchange frustration and transverse spin freezing in iron-rich metallic glasses *Phys. Rev.* B **51** 15885–97
[20] Ryan D H, Tun Z and Cadogan J M 1998 The ferromagnet to spin-glass cross-over: a neutron depolarisation study *J. Magn. Magn. Mater.* **177–181** 57–62
[21] Beath A D and Ryan D H 2007 Coexistence of spin-glass and ferromagnetic order in the $\pm j$ Heisenberg spin-glass model *Phys. Rev.* B **76** 064410
[22] Thomson J R, Guo H, Ryan D H, Zuckermann M J and Grant M 1992 Magnetic ordering in the three-dimensional frustrated Heisenberg model *Phys. Rev.* B **45** 3129–32
[23] van Lierop J and Ryan D H 2001 Spin dynamics in a frustrated magnet *Phys. Rev. Lett.* **86** 4390–3
[24] Liou S H, Xiao G, Taylor J N and Chien C L 1985 Magnetic properties and hyperfine interactions of amorphous Fe–Hf alloys *J. Appl. Phys.* **57** 3536–8
[25] Unruh K M and Chien C L 1984 Magnetic properties and hyperfine interactions in amorphous Fe–Zr alloys *Phys. Rev.* B **30** 4968–74
[26] Liou S H and Chien C L 1987 Composition range of binary amorphous alloys *Phys. Rev.* B **35** 2443–6
[27] Webb T A, Nikkinen L, Gallego J and Ryan D H 2013 A simple digital TDPAC spectrometer *Hyperfine Interact.* **222** 103–8
[28] Webb T A and Ryan D H 2013 Observation of transverse spin freezing by TDPAC *Hyperfine Interact.* **221** 1–5

[29] Béraud R, Berkes I, Danière J, Marest G and Rougny R 1969 Effect of finite time-resolution on perturbed angular correlation measurements *Nucl. Instrum. Methods* **69** 41–4
[30] Handrich K 1969 A simple model for amorphous and liquid ferromagnets *Phys. Status Solidi* **32** K55–8
[31] Ryan D H, Cadogan J M and van Lierop J 2000 Muon spin resonance study of transverse spin freezing in a-Fe_xZr_{100-x} *Phys. Rev.* B **61** 6816–20
[32] Ryan D H, van Lierop J, Pumarol M E, Roseman M and Cadogan J M 2001 Muon spin relaxation examination of transverse spin freezing *J. Appl. Phys.* **89** 7039–43
[33] Ryan D H, Coey J M D and Ström-Olsen J O 1987 Magnetic properties of iron-rich Fe–Hf glasses *J. Magn. Magn. Mater.* **67** 148–54
[34] Ryan D H, van Lierop J, Pumarol M E, Roseman M and Cadogan J M 2001 Field dependence of the transverse spin freezing transition *Phys. Rev.* B **63** 140405(R)
[35] Moorjani K and Coey J M D 1984 *Magnetic Glasses* (*Methods and Phenomena* vol 6) (Amsterdam: Elsevier)
[36] Bakonyi I 2005 Atomic volumes and local structure of metallic glasses *Acta Mater.* **53** 2509–20
[37] Baudry A and Boyer P 1987 Approximation of the Blume's stochastic model by asymptotic models for PAC relaxation analysis *Hyperfine Interact.* **35** 803–6
[38] Park T, Hodges J A, Moreno C, Stufflebeam M, Evenson W E, Matheson P, Zacate M O and Collins G S 2011 Relating PAC damping to EFG fluctuation rates through the PAC relaxation peak *Hyperfine Interact.* **199** 397–402